Polyaniline nanowire arrays generated through oriented mesoporous silica films: effect of pore size and spectroelectrochemical response

Wahid Ullah, Grégoire Herzog, Neus Vilà, Alain Walcarius

Polyaniline nanowire arrays generated through oriented mesoporous silica films: effect of pore size and spectroelectrochemical response

Wahid Ullah,[a] Grégoire Herzog,[a] Neus Vilà[a] and Alain Walcarius*[a]

Received (in XXX, XXX) Xth XXXXXXXXX 20XX, Accepted Xth XXXXXXXXX 20XX
DOI: 10.1039/b000000x

Indium-tin oxide electrodes modified with vertically aligned silica nanochannel membrane have been produced by electrochemically assisted self-assembly of cationic surfactants (cetyl- or octadecyl-trimethylammonium bromide) and concomitant polycondensation of the silica precursors (tetraethoxysilane). They exhibited pore diameters in the 2-3 nm range depending on the surfactant used. After surfactant removal, the bottom of mesopores was derivatized with aminophenyl groups via electrografting (*i.e.*, electrochemical reduction of *in situ* generated aminophenyl monodiazonium salt). These species covalently bonded to the ITO substrate were then exploited to grow polyaniline nanofilaments by electropolymerization of aniline through the nanochannels. Under potentiostatic conditions, the length of polyaniline wires is controllable by tuning the electropolymerization time. From cyclic voltammetry characterization performed either before or after dissolution of the silica template, it appeared that both the polyaniline/silica composite and the free polyaniline nanowire arrays were electroactive, yet with much larger peak currents in the latter case as a result of larger effective surface area offered to the electrolyte solution. At identical electropolymerization time, the amount of deposited polyaniline was larger when using the silica membrane with larger pore diameter. All polyaniline deposits exhibited electrochromic properties. However, the spectroelectrochemical data indicated more complete interconversion between the coloured oxidized form and colourless reduced polyaniline for the arrays of nanofilaments in comparison to bulky films. In addition, the template-free nanowire arrays (*i.e.*, after silica dissolution) were characterized by faster electrochromic behaviour than the polyaniline/silica hybrid, confirming the potential interest of such polyaniline nano-brushes for practical applications.

1. Introduction

Ordered mesoporous materials hold a prominent position in electrochemistry,[1] notably because of their attractive features (very large surface areas offering huge amounts of active sites, widely-open regular structure ensuring fast transport properties, hosting ability for the immobilization of (electro)catalysts or (bio)molecules, for instance), which can be exploited primarily in the field of electrochemical sensors and biosensors,[1-4] or for energy conversion and storage.[1,5-7] Electroanalytical applications involved mainly nanomaterials based on either mesoporous carbon[8-11] or mesoporous silica.[12-14] Silica-based materials are insulating but offer the versatility to be easily functionalized with a wide range of organic groups covalently bonded to the internal surfaces of mesopore channels.[15-17] Among the various morphologies available for mesoporous silica and organically modified silicates, thin films appear as very appealing in various fields,[18-20] including electrochemistry.[1] An important parameter that must be taken into account to ensure good performance in many applications is the accurate control of pore orientation, which is ideally obtained with uniaxially oriented one-dimensional (1D) mesopore channels.[21]

Mesoporous silica thin films made of vertically aligned nanochannels with respect to the underlying electrode surface are indeed attractive for electroanalytical purposes.[14,22-25] They can be produced by electrochemically assisted self-assembly (EASA, combining the sol-gel process with electrochemically driven cooperative self-assembly of surfactant micelles onto an electrode surface),[26,27] a Stöber solution growth mechanism,[28] an oil-induced co-assembly process,[29] or other approaches.[30-32] The EASA method is very fast and versatile, leading always to a high level of hexagonal packing of perpendicularly oriented mesopore channels of typically 2-3 nm in diameter,[27,33] and enabling also the attachment of organo-functional groups onto the silica walls.[34] These oriented nanoporous membranes on electrodes exhibit permselective behaviour based on both size and charge selectivities,[25] which can be otherwise tuned by adjusting the pore diameter,[35] the solution pH or ionic strength,[36-38] or via appropriate derivatization of the films.[39-41] When functionalized with redox-active moieties, the vertical nanochannels become the theater of unidirectional charge transfers by long-range electron hopping through the insulating silica membrane,[35,42-45] with more effective charge percolation than on other types of mesostructures.[46] Finally, such oriented mesoporous silica films are attractive hosts for confinement of reagents (nano-objects, nano-sized materials or supramolecular assemblies).[44,47,48] They are also, in principle, ideal hard templates for the growth of nanofilaments with ultra-small diameters, but this is quite challenging as demonstrated for metal nanowires electrodeposition, for instance.[49] Yet, the generation of organic polymers by electropolymerization through vertically ordered mesoporous silica-nanochannel film appeared to be feasible,[50-60] but care has to be made to restrict the polymer growth to the nanochannels length (*i.e.*, not outside the film) and to ensure the durable binding of polymeric nanofilaments to the underlying electrode surface (if wishing to remove the silica hard template for further use as polymer nanowire arrays).

The first attempts to generate polymeric nanostructures within vertically oriented silica mesochannels as hard template have been reported for conducting polymers such as polythiophene[50] or related derivatives,[51,52] polypyrrole,[53] polyaniline,[54] or polyquinone.[55] If the electropolymerization process was indeed expected to start onto the area of the electrode surface located at the bottom of mesopore channels, and polymer chains to grow from this area in the direction of the nanochannels, the resulting polymeric nanowires observed by microscopy exhibited diameters much larger than the mesopore diameters,[50,56] suggesting a growth out of the mesoporous membrane. Only with careful control of the electropolymerization conditions (notably the deposition time), it was possible to get polymer chains confined only in the mesopore channels, as reported for polyaniline (PANI).[54,57] However, upon dissolution of the silica template, PANI nanostructures did not stick onto the electrode surface, leaching out themselves in the form of broken pieces of polymer.[54] This therefore did not allow their use as arrays of "free" nanowires attached to the electrode surface (even if such PANI nanofilaments were indeed electroactive once entrapped in the silica membrane[54,57]). A way to improve their adhesion/linkage to the electrode material is the prior deposition of a layer of the polymeric material (i.e., as bulk coating) before the generation of the mesoporous silica membrane and subsequent electropolymerization, so that the polymeric nanowires are expected to bind to the bulk coating of the same composition, even after template removal (as exemplified for poly(3,4- ethylenedioxythiophene,[58] polyquinone[59] or polypyrrole[56]). Nevertheless, the resulting materials are actually made of two parts (underlying bulky coating and overlying wires) so that the response of the modified electrodes would be not only due to the individual nanofilaments. Note that arrays of single PANI nanowires/nanorods can be generated otherwise, but their lowest diameters are restricted down to ten or some tens of nanometers depending on the template approach used for their synthesis.[61-63] In a preliminary communication,[60] we have proposed a way to circumvent the above limitations, based on the covalent binding of aniline moieties onto the electrode surface prior to electropolymerization of PANI through the vertically aligned silica nanochannels, so that the resulting PANI nanofilaments remain chemically attached to the electrode support after removal of the mesoporous template.

In the present work, we have extended the approach to the generation of PANI nanofilaments covalently attached to indium-tin oxide (ITO) electrodes by using vertically oriented mesoporous silica template with two distinct pore diameters (in the 2-3 nm range) and investigated their respective electrochemical behaviour and spectroelectrochemical response. The materials preparation involved first the deposition of the mesoporous silica film by EASA on ITO using a surfactant as structure-directing agent (cetyl- or octadecyl-trimethylammonium bromide), then the electrografting of aminophenyl diazonium cations, and finally the electropolymerization of aniline to grow the PANI nanofilaments through the vertically aligned nanochannels. The electropolymerization process was monitored by recorded *i-t* curves during the potentiostatic deposition while the electrochemical behaviour of the resulting PANI nanostructures was analysed by cyclic voltammetry respectively before and after removal of the silica template. The obtained PANI nanofilaments exhibited attractive electrochromic properties resulting from fast interconversion between oxidized and reduced forms, which was extremely stable for the template-free materials.

2. Experimental section

2.1. Chemicals and reagents

Tetraethoxysilane (TEOS, 98%, Alfa Aesar), ethanol (95-96% Merck), $NaNO_3$ (99%, Fluka), HCl (Riedel de Haan, 1 M solution), cetyltrimethyl ammonium bromide (CTAB, 99%, Acros) and trimethyloctadecyltrimethylammonium bromide (ODAB; 98% Sigma Aldrich) were used for mesoporous silica film synthesis. All reagents for electrografting were purchased from Sigma Aldrich and used as received: *p*-phenylenediamine (98%), $NaNO_2$ (≥97%) and HCl (37%). PANI electropolymerization was performed using aniline (99.5%, Sigma Aldrich), which was distilled under vacuum before use. H_2SO_4 (98%, Sigma) was used as electrolyte for the electrochemical characterization of PANI. NaOH (VWR International) was used for silica template dissolution. All solutions were prepared with high purity water (18.2 MΩ cm^{-1}) obtained from a Purelab Option-Q from ELGA.

2.2. Preparation of vertically aligned mesoporous silica thin films

The mesoporous silica films with pore diameters of 2.0 and 2.9 nm (Figure 1) were prepared by electrochemically assisted self-assembly on ITO plates (surface resistivity 8-12 Ω, from Delta Technologies) as described elsewhere.[35] Briefly, typical sols were prepared from mixing in 1:1 v/v ratio an ethanol solution containing 100 mM of the silica precursor, TEOS, and an aqueous medium made of 32 mM of the surfactant (CTAB or ODAB) in the presence of 0.1 M $NaNO_3$ as electrolyte. After adjusting pH at 3 (by adding the necessary amount of 1 M HCl), the sol solutions were hydrolysed under stirring at room temperature for 2.5 hours, and then used as electrodeposition medium for the preparation of vertically aligned mesoporous silica films. This was achieved by applying a potential of -1.3 V for 20 s at the ITO working electrode (8 mm in diameter) in contact to the aged sol. After film formation, the electrodes were treated overnight at 130 °C (to ensure good cross-linking of the silica network). Removal of the surfactant species was performed using 0.1 M HCl in ethanol, as previously described.[27]

2.3. Generation of PANI nanofilaments

An aqueous solution containing 5 mM *p*-phenylenediamine and 5 mM $NaNO_2$ in 0.5 M HCl was first prepared and allow to react for 10 min under stirring in order to produce aminophenyl monodiazonium cations. These *in situ* generated species were then electrochemically reduced (typically at -0.2 V for 1 min) using ITO electrodes covered with the vertically aligned mesoporous silica films in order to attach covalently aminophenyl groups on the ITO surfaces located at the bottom of mesochannels. The grafted electrodes were then rinsed with water and sonicated for 5 min in ethanol to remove the unreacted diazonium species. PANI nanofilaments were generated by exposing the

electrode surface (5 mm in diameter) to a solution of 0.1 M aniline (in 0.5 M H_2SO_4) and performing electropolymerization typically under potentiostatic conditions (at +0.85 V for selected periods of time).[60] The same experiments were also carried out with bare ITO electrodes for comparison purposes. In order to get template-free PANI nanofilaments, the mesoporous silica film was dissolved by chemical etching in 1 M NaOH (10 min).

2.4. Apparatus and procedures for materials characterization

All electrochemical experiments (mesoporous silica film synthesis, electrografting, electropolymerization, cyclic voltammetry (CV) characterization and spectroelectrochemical measurements) were performed with a PGSTAT 100 or a µAutolab from Ecochemie (Metrohm, Switzerland) operated by NOVA software (Autolab). Three kinds of three-electrode cells were used: a first homemade one for film synthesis, made of ITO working electrode, a silver rod as pseudo-reference electrode and stainless steel counter electrode;[35] a second homemade one for electrografting, electropolymerization and cyclic voltammetry; made of modified ITO working electrodes, an Ag|AgCl|1 M KCl reference electrode (purchased from Metrohm, Switzerland) and a stainless steel rod as counter electrode; and a third one commercially available (the liquid transmission spectroscopy "Omni-Cell" from SPECAC, UK) adapted to host our modified ITO plates as working electrodes, along with Ag|AgCl wire as reference electrode and a platinum grid as counter electrode. UV-visible spectra were recorded using the Cary 60 UV-Vis spectrometer (Agilent Technologies). Transient profiles of absorbance variations were recorded at a wavelength of 750 nm upon successfully interchanging PANI between its oxidized to reduced forms, by applying alternatively +0.3 V and -0.2 V to the working electrode.

The mesoporous films were observed by transmission electron microscopy (TEM) using a JEOL ARM200F cold FEG TEM/STEM apparatus equipped with GIF Quantum ER (after mechanically removing portions of the film from the ITO surface). The film mesostructure was also analysed by grazing-incidence small-angle X-ray scattering (GISAXS), by collecting data on a "SAXSess mc²" instrument (Anton Paar) equipped with Cu-Ka source (λ = 0.1542 nm) operating at 40 kV and 50 mA and a CCD detector (Princeton Instruments).

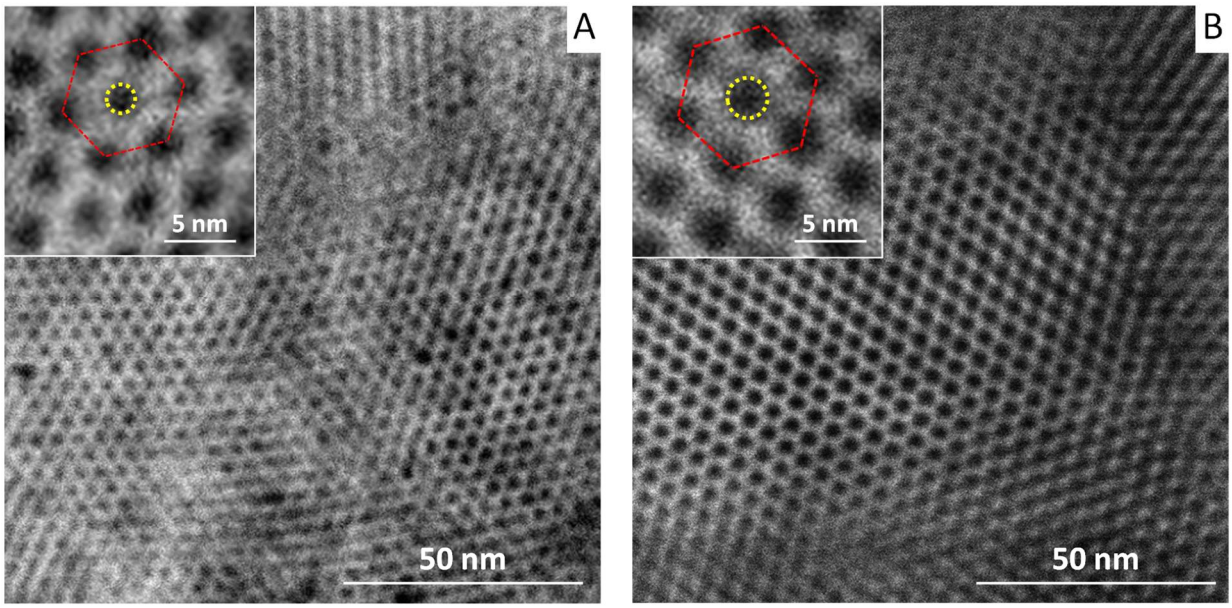

Figure 1. Transmission electron micrographs (top views) of the ordered and oriented mesoporous silica films prepared by EASA on ITO electrode using respectively CTAB (A) and ODAB (B) as structure-directing agents.

3. Results and Discussion

3.1. Generation of PANI nanofilaments by combining electrografting and electropolymerization

Figure 2A illustrates schematically how arrays of PANI nanofilaments were generated onto ITO. First, a mesoporous silica film made of vertically aligned hexagonally-packed nanochannels was generated by the nowadays well established EASA method,[27] involving the application of a cathodic potential likely to induce the self-assembly of cationic surfactants onto the electrode surface and concomitant gelification of the sol solution upon electrochemically triggered pH increase, leading to the growth of a silica mesopore channels network oriented perpendicularly to the underlying support. In a second step, aminophenyl groups were electrografted onto the ITO surface areas located at the bottom of the nanochannels, by reduction of the corresponding monodiazonium cations generated *in situ*,[60,64,65] via a mechanism given on the left bottom part of Figure 2A. The electrografting process can be induced and follow by cyclic voltammetry (Figure 2B). Figure $2B_1$ shows the CV curves obtained for the electrochemical reduction of the monodiazonium cations of *p*-phenylenediamine, with the characteristic peak appearing at -0.08 V(vs. Ag/AgCl) corresponding to the formation of the aryl radicals

expected to bind to the electrode surface. Its intensity decreased on the second cycle as a result of the partial coverage/passivation of the ITO surface grafted with the aminophenyl groups. The presence of these latter can be also evidenced by CV (Figure 2B$_2$), showing their characteristic irreversible oxidation signal around +1.0 V,[60,64] and an additional smaller one at lower potential values originating most probably from free oligomers.[65,66] Electrografting can be also performed potentiostatically, at -0.2 V for 1 min, as previously optimized.[60]

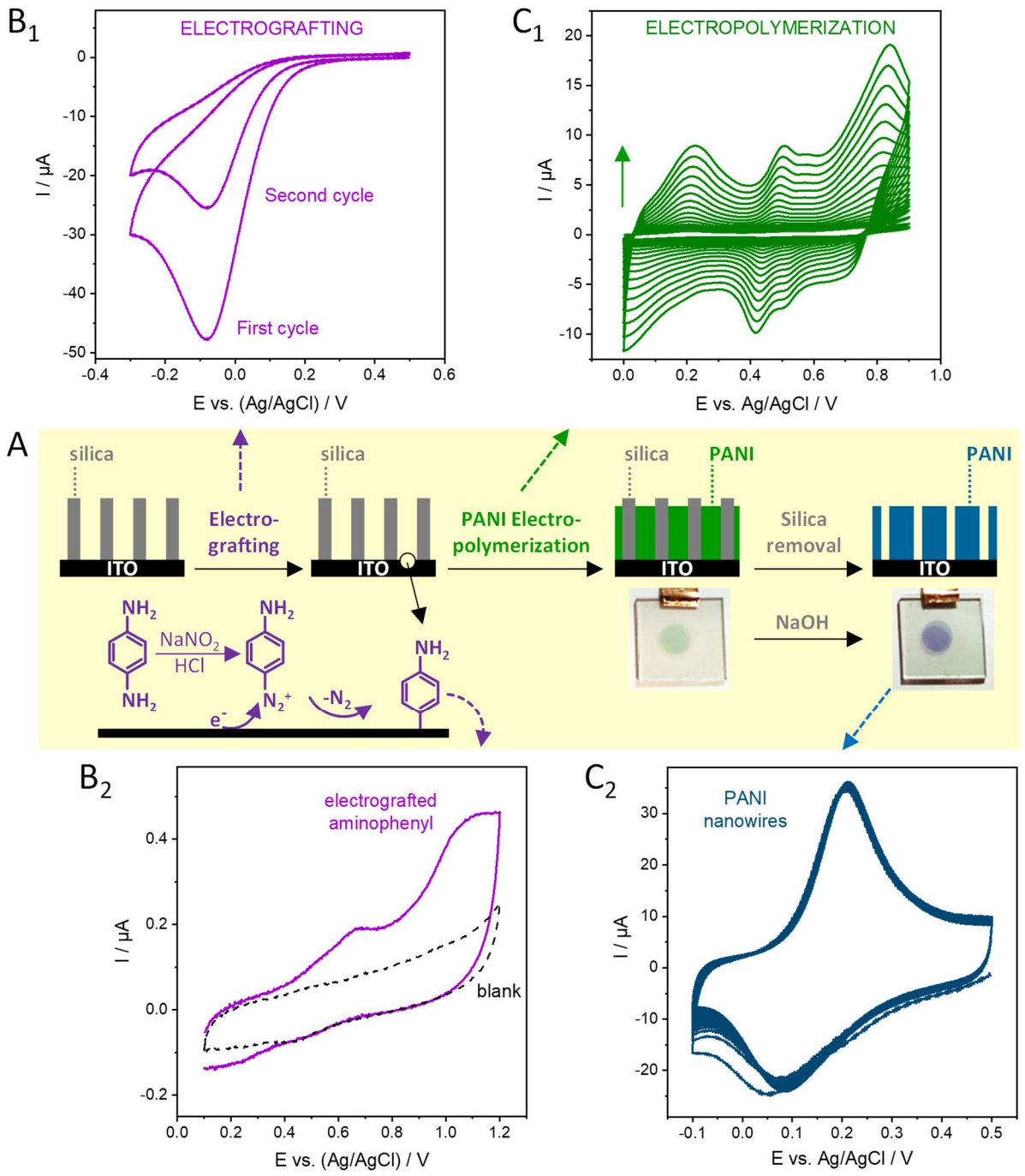

Figure 2. (A) Illustration of the generation of PANI nanofilaments on ITO electrode, using a vertically aligned mesoporous silica membrane as hard template, by combining electrografting of the monodiazonium salt of *p*-phenylenediamine and electropolymerization of aniline, with subsequent removal of silica to get the template-free nanofilaments (photos of the deposits are also shown). (B) Typical CVs related to the electrografting step: (B$_1$) two successive CVs recorded at 50 mV s^{-1} in 5 mM *p*-phenylenediamine + 5 mM $NaNO_2$ (in 0.5 M HCl) using the mesoporous silica-modified ITO electrode; (B$_2$) CVs recorded at 20 mV s^{-1} in 0.5 M H_2SO_4 using the same modified ITO electrode electrografted with aminophenyl groups (blank = CV curve recorded without electrografting). (C) Typical CVs related to the electropolymerization step: (C$_1$) CV curves (20 cycles) recorded at 50 mV s^{-1} in 0.1 M aniline (in 0.5 M H_2SO_4) using the same electrode as for (B$_1$); (C$_2$) 100 consecutive CV scans recorded at 50 mV s^{-1} in 0.5 M H_2SO_4 using an ITO electrode with attached PANI nanofilaments.

In a third step, PANI electropolymerization was performed in an aniline solution (in H_2SO_4 medium) and CV was used to follow the process (Figure 2C). If performed in potentiodynamic conditions, the electropolymerization resulted in continuous growth of voltammetric signals in the 0.0-0.9 V potential window (Figure 2C$_1$), which are characteristics for the formation of polyaniline (*i.e.*, oxidation/reduction peaks for leucoemeraldine/emeraldine around 0.2 V and for emeraldine/pergraniline close to 0.8 V, with some additional signals in-between arising from by-products[66,67]). The growth was rather slow during the first 6-7 CV cycles and then much faster, suggesting two kinetic regimes, but this will be discussed more quantitatively when performing electropolymerization in a potentiostatic mode (see section 3.2).

The silica template can be removed by treating the electrode in NaOH medium and, thanks to the electrografted aminophenyl moieties acting as a molecular glue between the ITO surface and PANI, the nanofilaments stayed attached to the electrode (see the remaining coloured deposits on bottom right part of Figure 2A), the difference in colour originating from the deprotonation of emeraldine salt (green) to form emeraldine base (blue) at high pH values.[68,69] If performing the same treatment for PANI nanofilaments produced on an ITO surface that was not previously derivatized with aminophenyl groups, they were lost in solution, confirming the importance of the diazonium electrografting to ensure their covalent bonding to the underlying electrode substrate.[60] The durable attachment of PANI nanofilaments to the ITO electrode surface is also supported by the multiple successive CV scans performed in the potential window corresponding to the redox processes of the leucoemeraldine/emeraldine system, showing very reproducible peak currents for 100 consecutive cycles (Figure 2C$_2$), confirming moreover the reversible transformation of PANI chains between their undoped and doped forms.

The film analysis by GISAXS (Figure 3) indicated a high level of mesostructural order over wide areas of the silica membranes, with 2D GISAXS patterns exhibiting scattering spots in the equatorial plane, which is indicative of the unique vertical orientation of the nanochannels onto the ITO surface as typical for mesoporous silica thin films generated by EASA.[70] These spots arose from scattering of the (10) plane of the mesopore arrays, which appeared as peaks in the 1D GISAXS traces (see insets in Figure 3); for ODAB-based films, one can even notice the signals of (11) and (20) planes of the hexagonal mesostructured, confirming the high level of structural order. From values of scattering maxima (q_{max} = 1.70 ± 0.02 nm^{-1} for CTAB films and 1.55 ± 0.01 nm^{-1} for ODAB films), one can calculate *d*-spacings of 3.69 nm and 4.05 nm for the films respectively prepared from CTAB and ODAB surfactants. Considering the hexagonal packing of nanochannels, the pore-to-pore distances were evaluated at 4.26 nm and 4.68 nm, respectively, in agreement with TEM data (Figure 1). These observations are consistent with previously reported GISAXS characterization of such oriented films of distinct mesopore diameters.[33]

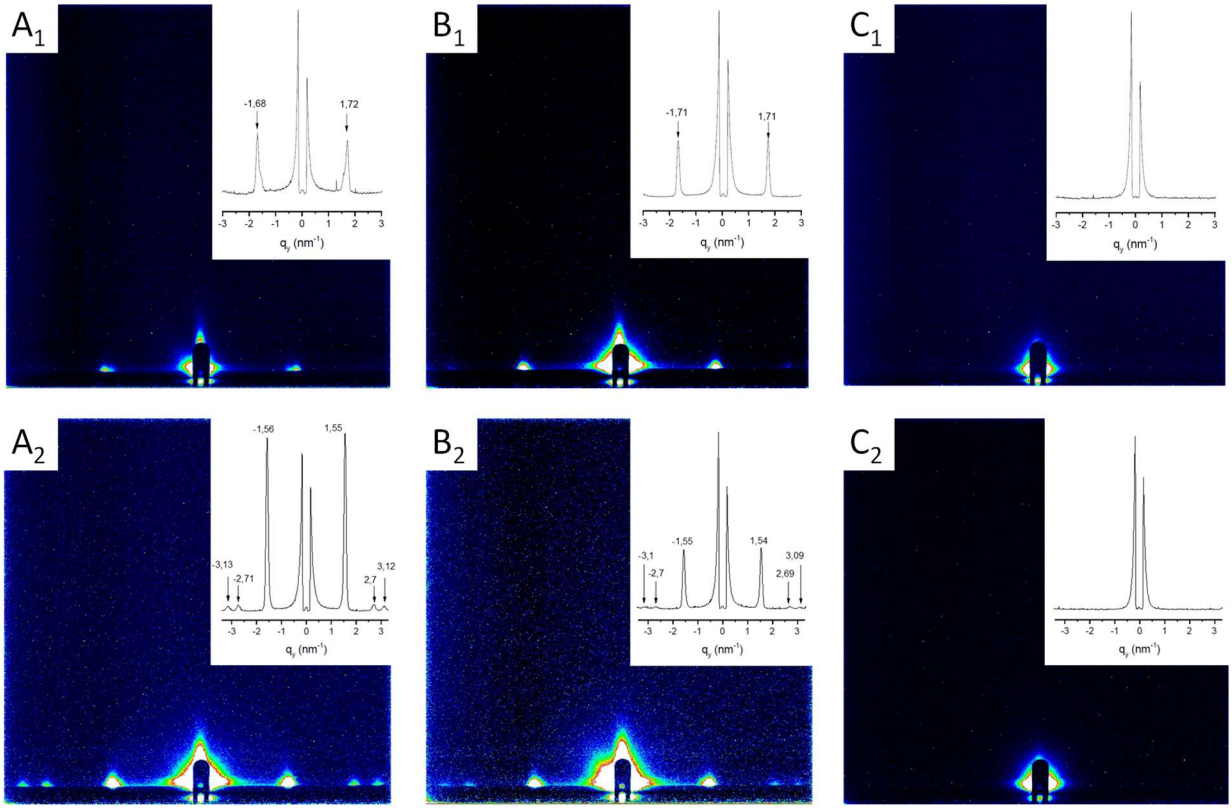

Figure 3. GISAXS patterns at the incidence angle of 0.25° and corresponding fitting curves (inset) for (A) ITO electrodes covered with the oriented mesoporous silica films and electrografted aminophenyl groups, (B) same electrodes as in (A) after PANI electropolymerization (at +0.85 V for 140 s), and (C) same electrodes as in (B) after removal of the silica template (in 1 M NaOH). The subscripts 1 and 2 corresponds to the films prepared from CTAB and ODAB surfactants, respectively.

The films mesostructure was maintained after PANI electropolymerization through both CTAB and ODAB films without any significant change in scattering parameters (compare parts A and B in Figure 3). Interestingly, the structure of the mesoporous PANI/silica composite films remained intact after long time storage in air (*i.e.*, same GISAXS patterns as in Figure 3B obtained after 1 year), suggesting a stabilizing effect of PANI wires (by contrast, the structure of bare mesoporous silica films with empty pores deteriorated within few weeks). However, after removal of the silica template, if one can be sure that PANI nanofilaments were still attached durably to the ITO surface and electroactive (Figure 2C$_2$), the corresponding GISAXS patterns did not show any noticeable scattering signal (Figure 3C), suggesting either some flexibility of such wires of ultra-small diameter or the lack of sensitivity of the GISAXS method to evidence any organization of so small organic filaments.

3.2. Effect of pore size and electrochemical characterization

PANI electropolymerization can be basically performed by cycling potentials in an appropriate window (typically between 0 and 1 V) or by applying a constant anodic potential (typically 0.8-0.9 V), the amount of deposited polymer being related respectively to the number of CV scans or to the time afforded for the application of the fixed potential. When operating with electrodes covered with a mesoporous silica film, the potentiostatic (or galvanostatic) methods are usually preferred because they enable a better control of the electropolymerized material.[54,57,60] Especially, the potentiostatic approach is suited to distinguish the growth rates for PANI generation in the mesopore channels and out of the silica membrane.[57,60] We therefore used this method to investigate the effect of mesopore diameter on the PANI growth process (Figure 4). Figure 4A shows the typical *I–t* curves obtained for the electropolymerization of aniline at +0.85 V (as optimized potential value for PANI growth through hard templates[57,60,71]) using ITO electrodes covered with mesoporous silica films with pore diameters of 2.0 nm (a) and 2.9 nm (b), which were previously grafted with aminophenyl groups. They exhibit the expected characteristic behaviour involving three steps: a first nucleation period (0-40 s) with rather low currents, then an increase of intensity (*ca.* 40-80 s) to reach almost plateau currents (*ca.* 80-120 s) that is related to the rate-determined growth of PANI wires through the mesochannels, and finally (above 120 s) steepy current variation corresponding to faster PANI growth outside the membrane on top of the mesoporous silica template. Only the short nucleation period and sharp current increase was observed for the control experiment performed on electrografted bare ITO (i.e., without silica film, see inset in Figure 4A), proving that plateau currents are indeed due to PANI growth through the mesopore channels. Times to reach current values equal to half of the plateau currents, $t_{1/2}$, were very similar independently on the pore diameter ($t_{1/2}$ = 63 s for ∅ = 2.0 nm and $t_{1/2}$ = 60 s for ∅ = 2.9 nm) and the plateau lengths were also very close to each other, suggesting similar confinement effects for the growth of nanofilaments. The main difference relied on the intensity of the plateau currents, which were slightly larger to the silica membrane with larger pore diameter compare curves (a) and (b) in Figure 4A). Integrating the *I–t* curves under the plateau gave rise to charges Q respectively equal to 1.7 and 2.1 mC. If considering the values of PANI electropolymerization efficiency (65%) and the number of electrons exchanged per aniline monomer during the electropolymerization process (2.7),[72] one can estimate the amounts of aniline units in the PANI grown in the silica membrane at about 2.5×10^{15} and 3.1×10^{15}, respectively for pore diameters of 2.0 nm and 2.9 nm. Taking into accounts the polyaniline density (1.33 g cm^{-3}),[68] these values would correspond to volumes of generated PANI of about 0.62×10^{-6} and 0.78×10^{-6} cm^3, respectively. When comparing these values to the available volume of mesopore channels (that one can estimate from the pore diameters obtained from TEM, the pore-to-pore distance from GISAXS, the nanochannel length equal to membrane thickness from profilometry measurements, and the exposed electrode area), one realized that PANI would occupy roughly between ½ and ⅓ of the pore volume. Figure 4B displays the CV curves recorded for these two samples after etching of the silica template. As shown, the larger peak currents observed with PANI filaments generated in the larger nanochannels confirms that the amount of electropolymerized PANI was larger in this case, consistent with the above observations from *I–t* curves (Figure 4A). Integration of the anodic signals gave values of 0.13 mC for the CTAB-based film (pore ∅ = 2.0 nm) and 0.22 mC for the ODAB-based film (pore ∅ = 2.9 nm). Considering that two aniline units are involved in the one-electron transfer process,[69] these values correspond to respectively 1.6×10^{15} and 2.7×10^{15} aniline units. If compared to the above amounts of electropolymerized material estimated from chronoamperometric data, it means that about 64% and 84% of the generated PANI were electrochemically accessible after etching of the silica membrane. The lower recovery value obtained for the nanofilaments prepared from the mesoporous film with smaller diameter can be due to some damage/loss of PANI during etching, as otherwise suggested previously for similar material deposited through very narrow nanochannels[54] When lengthening too much the electropolymerization (*e.g.*, for 160 s), PANI grew outside the film and one can observe it by SEM via a rather dense granular deposit on top of the smooth mesoporous silica film surface (compare parts (a) and (c) in Figure 4C), which is not present when stopping the polymer growth on the plateau (*i.e.*, $t_{\text{electropolymerim}}$ = 100 s) for which the surface state (see part (b) in Figure 4C) is almost the same as prior to electropolymerization (few silica beads are also noticeable, as common for mesoporous silica films produced by EASA[27]). The increasing amounts of grown PANI can be also evidenced with the naked eye, showing a progressively increasing colouration (Figure 4D), noticeable respectively before and after removal of the silica template with the characteristic colour change from green to violet/blue as aforementioned (bottom right part of Figure 2A). Note that the silica etching did not affect the mechanical stability or sticking of the PANI deposits, except when applying too long electropolymerization times (*e.g.*, for 180 s) for which the too large amounts of PANI were likely to be damaged during NaOH treatment (see bottom right of Figure 4D).

CV performed at various potential scan rates (Figure 5) was then used to characterize the electrochemical behaviour of PANI nanowire arrays obtained using ITO electrodes covered with mesoporous silica films with distinct pore diameters (*i.e.*, 2.0 and 2.9 nm) for different electropolymerization times selected from Figure 4A, corresponding to PANI filaments of variable length ($60 < t_{\text{electropolymerim}} < 120$ s) and one sample with additional PANI deposits onto the silica membrane (*i.e.*, $t_{\text{electropolymerim}}$ = 140-160 s). The CV curves were recorded

respectively before and after removal of the silica template. The left part (Figure 5A) corresponds to data obtained for the CTAB-based film (∅ pores = 2.0 nm) while the right part (Figure 5B) gathers those results originating from the ODAB-based film (∅ pores = 2.9 nm).

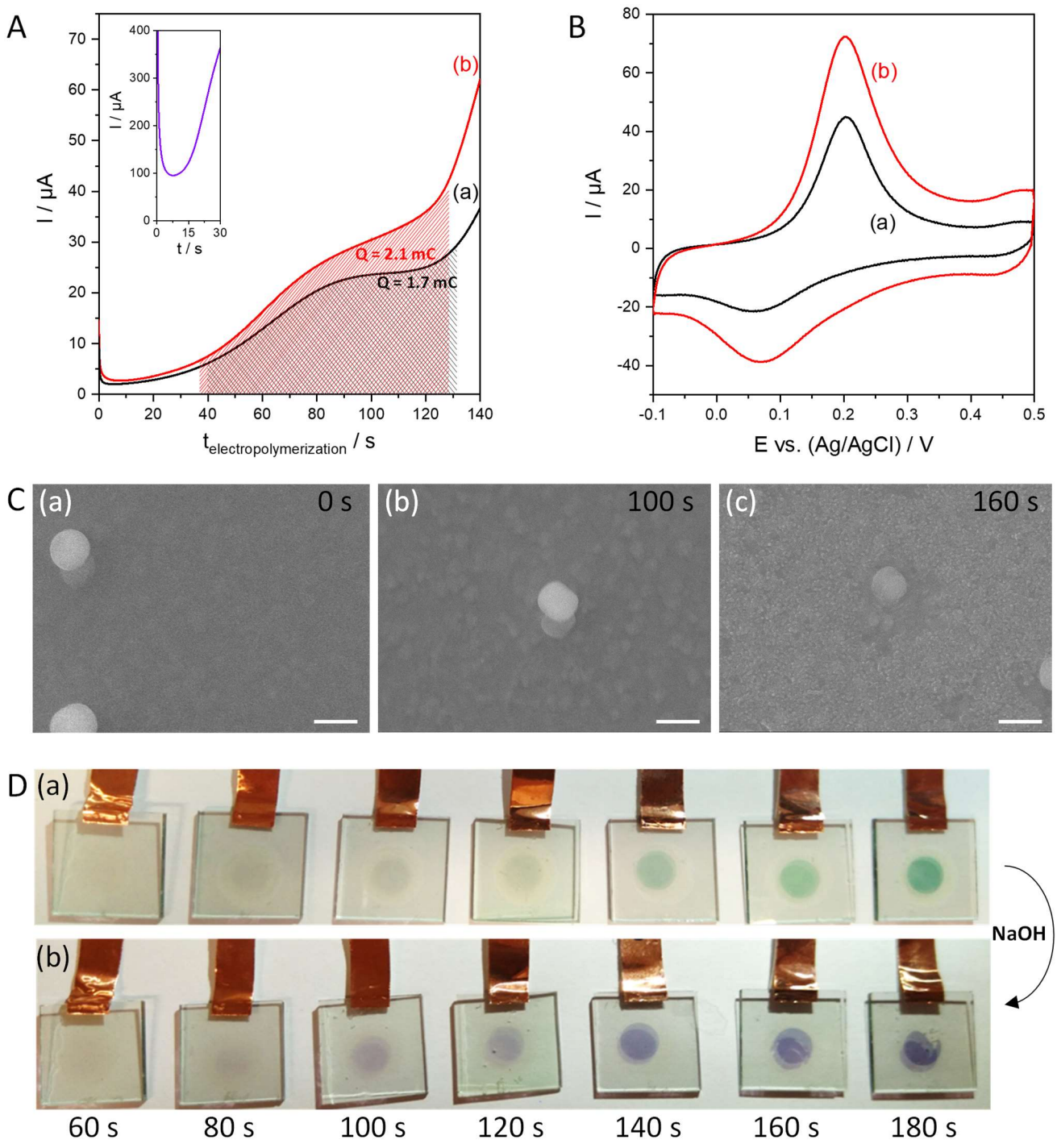

Figure 4. (A) *I* – *t* curves recorded during PANI electropolymerization in 0.1 M aniline (in 0.5 M H_2SO_4) at constant potential (+0.85 V) using ITO electrodes covered respectively with (a) CTAB- and (b) ODAB-based mesoporous silica films, which were previously electrografted with aminophenyl groups (the inset shows the curve obtained in the absence of mesoporous silica film). (B) Corresponding CVs recorded at 50 mV s^{-1} in in 0.5 M H_2SO_4 using the same electrodes as in (A) after removal of the silica template by chemical etching (in 1 M NaOH). (C) Typical SEM micrographs of the ITO/mesoporous silica film surface (scale bars = 500 nm), respectively before (a) or after 100 s (b) or 160 s (c) electropolymerization (CTAB-based films). (D) Photographs of the ITO/mesoporous silica film electrodes obtained after increasing times of PANI electropolymerization: (a) before and (b) after etching of the silica template, respectively.

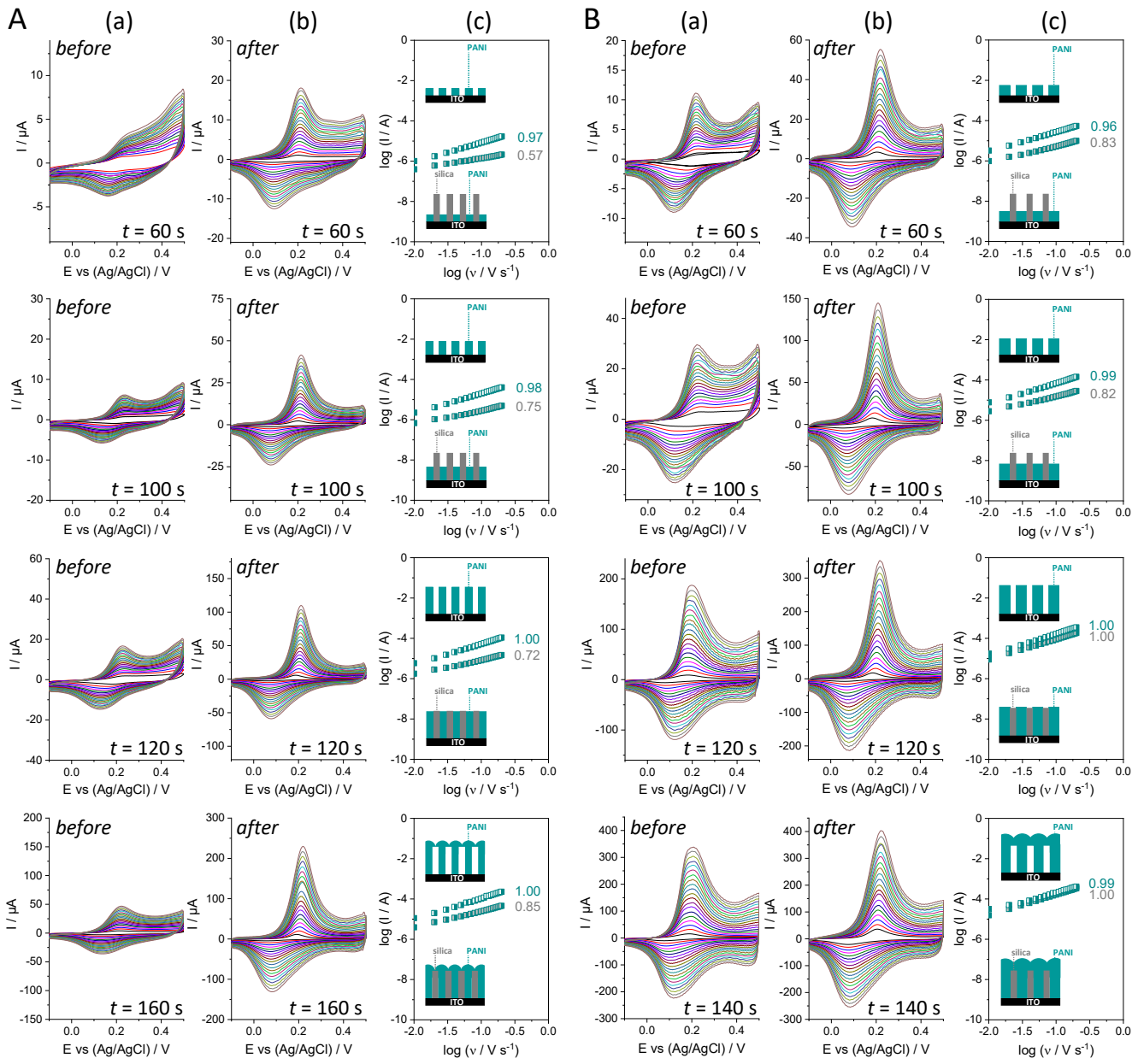

Figure 5. Cyclic voltammetry characterization of PANI nanowires generated through mesoporous silica films with pore diameters of (A) 2.0 nm and (B) 2.9 nm for various electropolymerization times (60, 100, 120, 140 or 160 s; see indication on plots) respectively (a) 'before' and (b) 'after' etching of the silica membrane; CV curves were recorded at various potential scan rates from 10 to 200 mV s^{-1} (every 10 mV s^{-1}). The variations of anodic peak currents versus scan rates (log-log scale) are shown on parts (c) of the figure (before and after template removal, with numbers representing the slopes of the linear fittings), along with schemes illustrating the expected extents of PANI filaments growth in each case.

General tendencies can be identified from these experiments. First, the CV signals corresponding to the leucoemeraldine/emeraldine redox processes visible in the investigated potential window (-0.1 to 0.5 V) were always more intense for samples prepared at longer electropolymerization times, evidently due to larger amounts of grown/deposited PANI material, and this trend was observed for both PANI/silica composites and silica-free PANI nanostructures. Peak currents were always located at the same potential values independently on the potential scan rate (yet with few exceptions at the very low 10-20 mV s^{-1} values), with anodic peaks at *ca.* 0.22 V for both material types whereas cathodic peaks shifted from 0.13 V to 0.08 V when PANI wires were free of the silica template. Secondly, the peak current intensities were always lower for PANI wires in the silica membrane than for the template-free samples (compare curves (a) "before" and (b) "after" silica removal in Figure 5). This can be rationalized in terms of larger surfaces of PANI exposed to the electrolyte solution after template etching. This effect was more marked for the silica films with narrower mesopores in which restrictions to transport phenomena are expected to be more important. It was however less marked at longer deposition times (*i.e.*, when PANI was formed on top of the

mesoporous film), especially for the larger pore template (see bottom of Figure 5), which can be explained by the whole electrode surface covered with PANI exposed to the electrolyte solution. Thirdly, the variations of peak currents, I_p, with the potential scan rate, ν, were investigated for all systems in order to determine the type of electrochemical behaviour (thin layer-confined or diffusion-controlled reactions). From the plots "log(I_p) vs. log(ν)", one can derive slopes (see parts (c) in Figure 5) which are expected to be equal to 0.5 for a purely diffusion-controlled process and to 1.0 for a purely thin layer response, and in-between for mixed behaviour. As one can see at first sight, all template-free samples (columns (b) and corresponding 'white-greenish square' data in columns (c) on Figure 5) are largely/exclusively dominated by thin layer-confined reactions, whereas the PANI-in-silica films (columns (a) and corresponding 'grey-greenish square' data in columns (c) on Figure 5) are characterized by some diffusion-controlled contributions, especially for the narrow mesopore diameter series and shorted electropolymerization times. To be more quantitative, one can consider that in case of mixed behaviour the overall current is the sum of contributions from thin layer (proportional to the scan rate) and from diffusion (proportional to the square root of scan rate):[73]

$$i = k_1\nu + k_2\nu^{1/2} \qquad (1)$$

where i is the current measured at a given potential (for example the peak potential), ν the scan rate, and k_1 and k_2 empirical parameters representing both contributions. Equation 1 can be normalized versus the square root of potential scan rate (equation 2) in order to extract the parameters k_1 and k_2 (respective percentages of thin layer and diffusion control) by plotting the variation of $i/\nu^{1/2}$ as a function of $\nu^{1/2}$.

$$\frac{i}{\nu^{1/2}} = k_1\nu^{1/2} + k_2 \qquad (2)$$

Accordingly, one always obtained thin layer contributions in the 99-100% range for all PANI nanofilaments after silica template removal, confirming a real interest of such ultra-small nanostructures for ensuring fast electron transfer processes, contrary to bulkier PANI deposits (even nanostructured ones) for which diffusion-controlled processes have been most often reported (as a result of rather slow counter-ions diffusion through the polymeric material).[71,74-76] For PANI wires in the silica membrane (*i.e.*, before etching), some contributions of diffusion-controlled reactions were evidenced (65%, 25%, 21% and 11%, respectively for PANI deposits at 60 s, 100 s, 120 s and 160 s in CTAB-based films, and 11% for both PANI deposits at 60 s and 100 s in ODAB-based films (and less than 1% for those PANI deposits at 120 s and 140 s with ODAB films)), confirming the above qualitative observations. Yet, the contributions of thin layer behaviour remained majority (except for the very short PANI nanofilaments prepared for 60 s in CTAB-based film), suggesting that even in so confined environments the electron transfer processes were quite fast and not significantly restricted by diffusion phenomena, consistent with the above estimation of PANI occupying roughly ½ – ⅓ of the mesopore section (keeping thus some space for easy mass transport of counter ions). The fast transport processes are also due to the unique vertical orientation of the nanochannels onto the electrode surface.[77,78]

3.3. Spectroelectrochemical characterization and electrochromic properties

The potential-dependent colouration/bleaching of PANI made it an attractive material for electrochromic applications.[79,80] However, the rigidity of PANI chains and the lack of access to aniline units in bulk polymer can hinder the transport of counter ions during doping/dedoping processes, undermining the electrochromic response. Among the strategies developed to overcome such limitations, one can cite the nanostructuration of PANI[71,74-76] or the design of PANI-based hybrid nanocomposites.[81-84] We have thus evaluated the possible interest of the PANI nanofilaments developed here as electrochromic materials. Focusing on the leucoemeraldine/emeraldine salt redox system, one can expect its transformation from a nearly transparent material with slightly yellowish tint in the reduced form to a greenish colour in the oxidized form. Figure 6 shows the absorbance spectra recorded for PANI electropolymerized through the mesoporous silica films for two selected polymerization times leading either to PANI nanofilaments only or to PANI nanofilaments and PANI deposits grown outside the films (see part A for CTAB-based films and part B for the ODAB-based ones), at applied potentials of -0.2 V and +0.3 V (corresponding respectively to the reduced and oxidized forms of the materials). In addition to the π-π* transition of the aromatic rings (visible at λ = 430-440 nm independently on the oxidation state of the polymer), the spectra recorded for the oxidized samples revealed a main band in the λ = 720-750 nm region corresponding to the polaron state of the green emeraldine salt state of PANI (yet with some minor contribution at λ values around 560-580 nm arising from the less conductive emeraldine base).[85] The intensity of this main band was larger for PANI electrogenerated for longer times as a result of larger amounts of polymer on the electrode surface, but the main information was the almost complete vanishing of this band when reducing the PANI deposits at -0.2 V only for the template-free samples (i.e., after removal of the silica membrane, compare red and black curves in parts (b) of Figure 6), suggesting more efficient electrochromic behaviour in this case. The non-negligible absorbance band remaining after reduction of PANI occluded in the silica matrix (see parts (a) of Figure 6) can be explained by less effective and slower redox processes, in agreement with the above CV data (Figure 5); this cathodic bias-induced change in the spectra was characterized by a red shift of absorbance towards higher wavelengths, consistent with previous reports.[54,81-83] Similar observations were made for both CTAB- and ODAB-based films. This constitutes a significant improvement with respect to bulk PANI layers for which the extent of bleaching was strongly limited by the existence of cross-linked and intertwined polymeric chains expected to induce conductivity loss and incomplete electrochemical reduction, contrary to the present PANI nanofilaments.[57]

Figure 7A shows typical *in situ* absorbance responses of (a) PANI/ITO and (b,c) PANI nanowires in mesoporous silica films (CTAB-type) on ITO respectively before (b) and after template etching (c), as measured at λ = 750 nm using a spectroelectrochemical cell containing the ITO working electrode biased successively at -0.2 V (bleaching step) and 0.3 V (colouration step) for 20 s per step (200 cycles). The absorbance change was larger for the bare ITO electrode covered with a bulky PANI layer (in comparison to PANI nanofilaments) but it decreased upon successive measurements probably due to some mechanical degradation of the material (one can see some losses of PANI

from such rather thick deposits). The stability was much better for PANI nanofilaments in the silica membrane, even if one can notice incomplete bleaching as measurements progressed, whereas perfect cyclability (no noticeable variation in absorbance changes between the 1st and 200th cycles). Enlarging the time window around one cycle enabled to evidence dramatic difference of response time depending on whether PANI nanofilaments were occluded in the silica membrane or template-free. For the example depicted in Figure 7A (parts (b) and (c)), an improvement by *ca.* one order of magnitude for colouration and almost two orders of magnitude for bleaching was observed when passing from the PANI/silica nanocomposite to the template-free PANI nanofilaments, and it was the case for all samples investigated here, independently on the diameters of the nanochannel membranes used to prepare the PANI wires (Table 1). This can be also observed when recording the absorbance responses continuously for increased and decreased bias (Figure 7B), showing an excellent and reversible dynamic for template-free PANI nanofilaments (b) in comparison to the PANI/silica nanocomposite film (a) for which bleaching was incomplete in the time scale of the experiment. Faster response times with template-free PANI nanofilaments is explained by faster redox switching between oxidized and reduced forms of PANI, in agreement with the above CV observations. The shortest response times obtained for the most efficient systems (i.e., 0.12 s for colouration and 0.10 s for bleaching with PANI nanofilaments electropolymerized for 120 s using CTAB-based template, and 0.11 s for colouration and 0.10 s for bleaching with PANI prepared for 100 s from ODAB-based template) are among the best ones in comparison to other PANI nanostructures.[71,74-76] Note that lengthening the electropolymerization time for PANI growth (i.e., up to reaching PANI deposits not only in the nanochannels but also on top of the silica membrane) resulted in response times of the same order of magnitude as for a bulk PANI layer on bare ITO and larger variations of absorbance, but it was at the expense of some lack of long-term stability especially after removal of the silica template (Table 1). A compromise has thus to be found, ensuring an amount of PANI deposits large enough to get a significant colouration efficiency with fast response time after template removal, but not too large to avoid problems related to possible degradation over prolonged used which could contribute to lack of long-term stability.

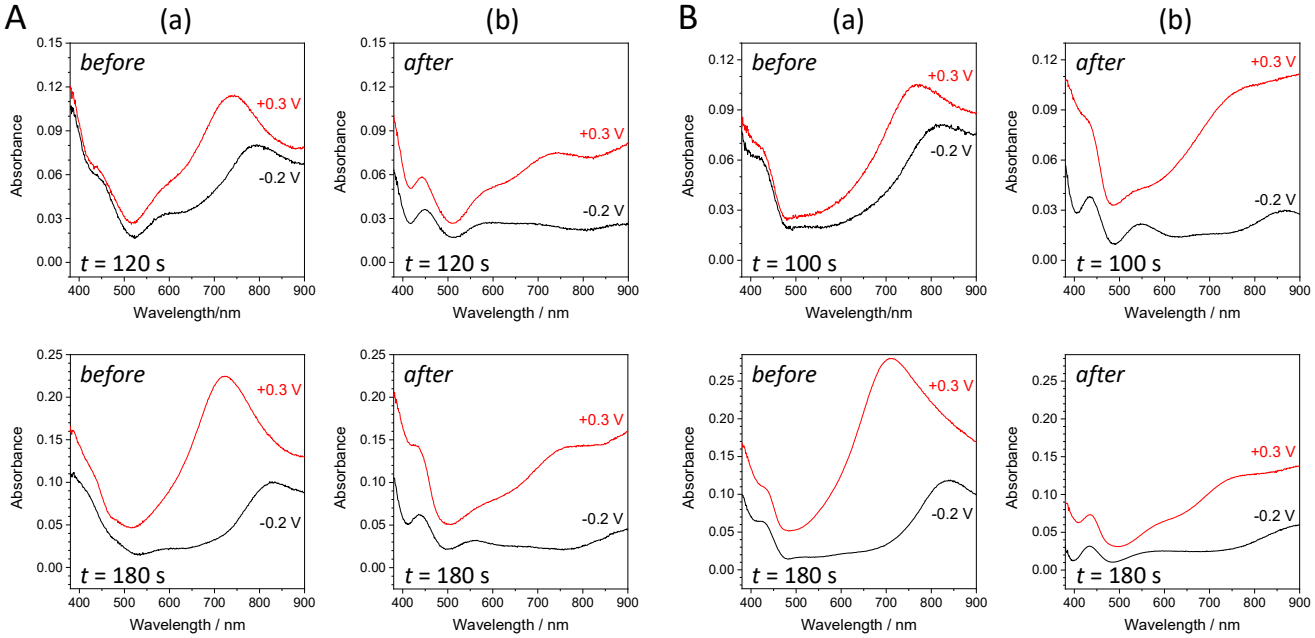

Figure 6. UV-vis spectra of the oxidized (+0.3 V) or reduced (-0.2 V) forms of PANI nanowires generated through mesoporous silica films with pore diameters of (A) 2.0 nm and (B) 2.9 nm for various electropolymerization times (100, 120 or 180 s; see indication on plots) respectively (a) 'before' and (b) 'after' etching of the silica membrane.

Table 1. Electrochromic characteristics of typical PANI materials investigated in this work (same conditions as in Figure 7A).

Samples		$t_{colouration}$ / s *	$t_{bleaching}$ / s *	$\Delta_{Absorbance}$	$\%_{response\ after\ 200\ cycles}$
PANI on bare ITO ($t_{electropolym}$ = 100 s)		1.1	1.2	0.25	56
PANI nanofilaments grown through CTAB-type films					
$t_{electropolym}$ = 120 s	*before template removal*	2.1	16.1	0.14	93
	after template removal	0.12	0.10	0.022	100
$t_{electropolym}$ = 180 s	*before template removal*	0.4	0.9	0.15	96
	after template removal	0.5	1.0	0.11	90
PANI nanofilaments grown through ODAB-type films					
$t_{electropolym}$ = 100 s	*before template removal*	1.8	14.4	0.06	84
	after template removal	0.11	0.10	0.038	99
$t_{electropolym}$ = 180 s	*before template removal*	0.6	2.6	0.17	98
	after template removal	0.3	2.0	0.10	86

* colouration and bleaching times measured at 95% of the maximum absorbance variations observed after application of +0.3 V and -0.2 V, respectively

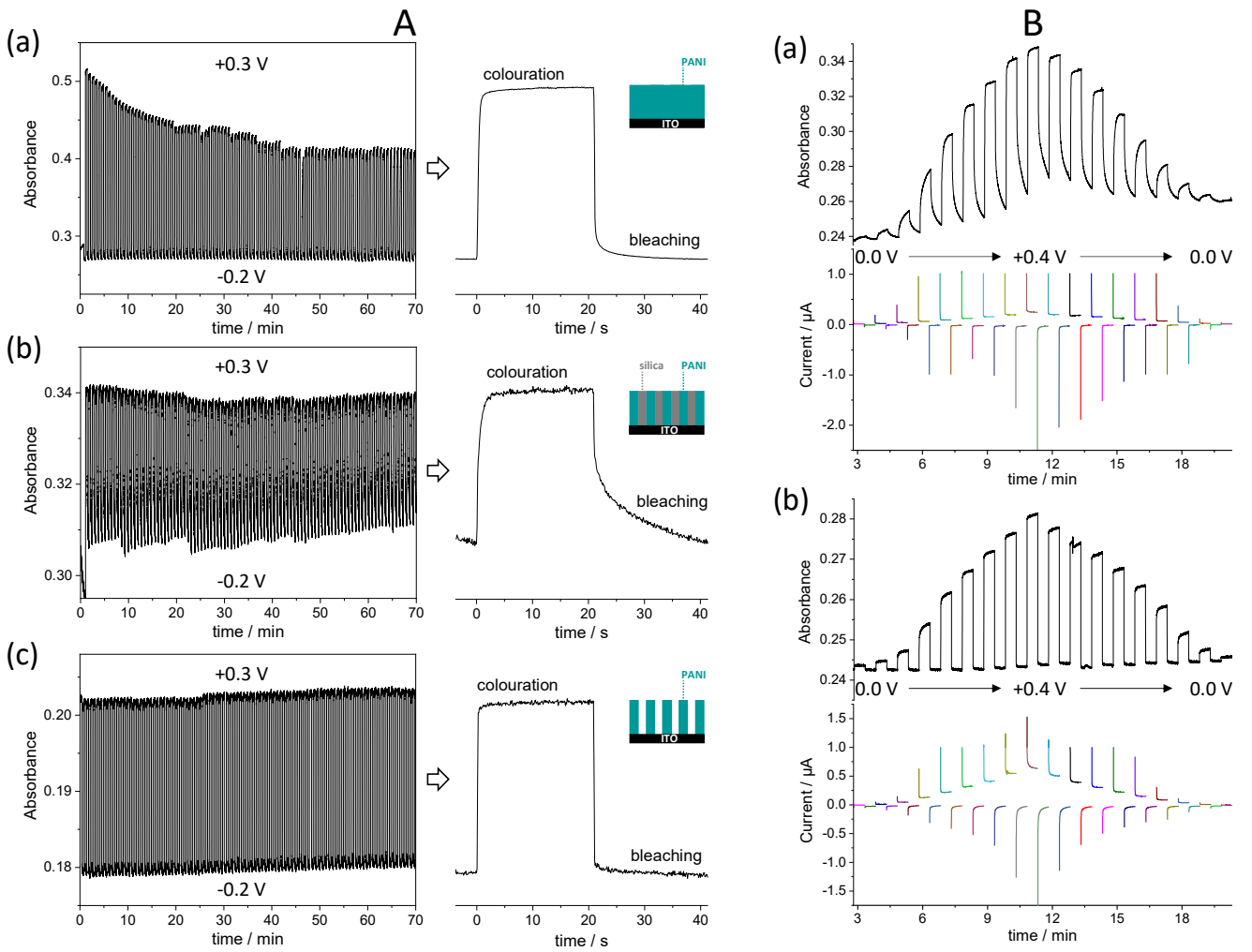

Figure 7. (A) Cycling stability at 750 nm (200 cycles at switching potentials of +0.3 V and -0.2 V; 20 s each) of PANI generated under 120 s electropolymerization on (a) bare ITO or (b,c) as nanofilaments grown through a mesoporous silica film (pore ∅ = 2.0 nm) on ITO electrode respectively (b) 'before' and (c) 'after' etching of the silica membrane (enlargement of one cycle on the right). (B) Effect of the applied potential on the spectroelectrochemical response of PANI nanowires, measured by switching potentials from -0.2 V to various anodic values (from 0.0 to +0.4 V, by steps of 50 mV), for samples obtained respectively (a) 'before' and (b) 'after' etching of the silica membrane.

3.4. Toward other applications?

Just to give an idea on what could be achieved next with such a forest of PANI nanofilaments, and considering the interest of PANI nanowire arrays for applications in the fields of electrocatalysis (i.e., for sensors[87-90]) or energy storage (e.g., as supercapacitors[89-92]), we provide hereafter some preliminary results in support of these possible applications.

Figure 8 shows the response of various electrodes to 1 mM ascorbic acid. On bare ITO electrode (curve a), no peak can be observed in the investigated potential range. When using PANI modified ITO electrodes, well-defined anodic signals were obtained, thanks to the catalytic properties of PANI for the oxidation of ascorbic acid.[93] However, the efficiency of the electrocatalytic process was strongly dependent on the electrode type. For PANI nanowires in mesoporous silica films (CTAB-type) on ITO before etching of the silica membrane (curve c), one observed a peak current of 61 µA located at +0.50 V, whereas the free nanofilaments gave rise to much better electrocatalytic response with a peak current of 280 µA located at +0.40 V (curve d). This is consistent with the more effective charge transport reported above for template-free PANI as a result of larger exposition to the electrolyte solution. The behaviour of an ITO electrode covered with a bulky PANI layer (prepared by electropolymerization on bare ITO with similar charge of for PANI nanofilaments) resulted in intermediate results (peak of 184 µA at +0.44V, see curve b), which can be due to less effective doping/dedoping processes in bulky PANI deposits than for PANI nanoarrays.[94] This highlights the attractiveness of 1D PANI nanofilament arrays for possible application in electrochemical sensing.

Figure 9 illustrates another possible application of PANI nanofilaments, i.e., as pseudocapacitive materials, showing typical triangle-shaped galvanostatic charge-discharge curves (Fig. 9A), with good cycling behaviour (over 1000 cycles) for both PANI nanofilaments in the silica

membrane and template-free wires (Fig. 9B&C). The areal specific capacitance values evaluated from the discharge curves were 1.30 and 2.35 mF cm^{-2} respectively before and after dissolution of the silica membrane, and 1.35 mF cm^{-2} for a bulk PANI film of the same amount of electropolymerized aniline units. For template-free PANI nanofilaments, the electrode surface is covered only with a very few amount of the polymer (i.e., 0.55 µg) and, if expressing the specific capacitance per mass of the material, one reached 427 F g^{-1} (at 9 A g^{-1}), which is comparable to PANI-graphene composites.[92] This material retained 64% of its initial specific capacitance after 500 cycles and 47% after 1000 cycles (Fig. 9C) whereas PANI nanowires in the mesoporous film before silica etching (Fig. 9B) were less stable (only 19% and 8% capacitance retention after 500 and 1000 cycles, respectively). These results have been obtained without any optimization and, in view of previous reports on redox-active mesoporous silica coatings prepared by EASA,[45,95] one can expect significant improvement when passing from a flat ITO support to electrode surfaces made of carbon nanomaterials, for instance.

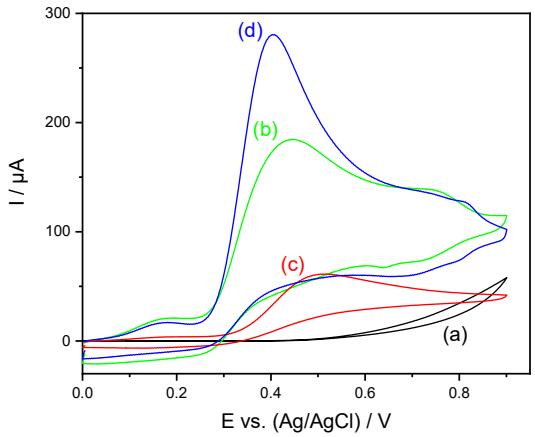

Figure 8. Cyclic voltammograms recorded in 1 mM ascorbic acid (in 0.1 M H_2SO_4) at a potential scan rate of 50 mV s^{-1}, using (a) a bare ITO electrode, (b) ITO covered with a bulky PANI film or (c,d) ITO modified with PANI nanowires generated through a mesoporous silica film with pore diameters of 2.0 nm for 120 s electropolymerization time, respectively (c) 'before' and (d) 'after' etching of the silica membrane. (b-d) PANI deposits correspond to an electropolymerization charge of 2.57 mC.

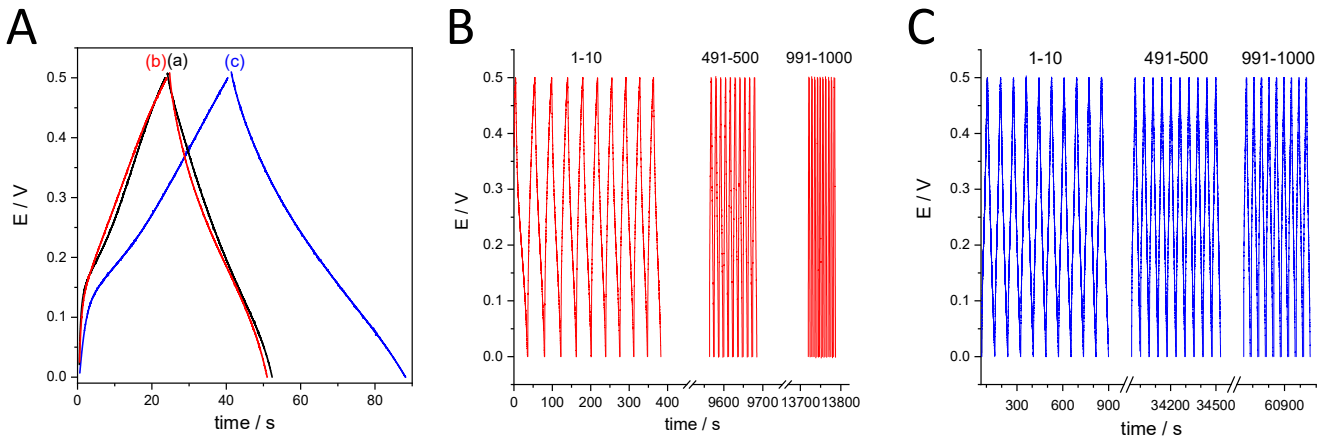

Figure 9. (A) Galvanostatic charge-discharge curves recorded in 0.5 M H_2SO_4 at a current density of 25 µA cm^{-2} using ITO electrodes respectively covered with (a) a bulky PANI film or (b,c) PANI nanowires generated through a mesoporous silica film with pore diameters of 2.0 nm ((b) 'before' and (c) 'after' etching of the silica membrane). (B,C) Charge-discharge profiles (10 first, 491-500th and 991-1000th cycles) for PANI nanowires prepared as in (A) and recorded in the same conditions, respectively (B) 'before' and (C) 'after' etching of the silica membrane. All PANI deposits correspond to an electropolymerization charge of 2.51 mC.

4. Conclusions

In this work, we have shown that one can control the growth of PANI nanofilaments through vertically aligned mesopore channels of silica films of distinct pore diameters (2-3 nm) generated by EASA onto ITO electrodes. Their durable attachment to the electrode surface (even after removal of the silica template) is achieved by electrografting aminophenyl groups at the bottom of the nanochannels prior to PANI

electropolymerization. The growth rate and the amount of deposited PANI were larger when using the silica membrane with larger pore diameters, resulting therefore in more intense CV responses. Both PANI nanofilaments in mesoporous silica and after etching of the membrane were electrochemically accessible, but peak currents were significantly larger after template removal owing to wider exposure of the polymer to the electrolyte solution. This had also an effect on the electrochromic properties of the materials, showing significantly improved response times for PANI nanofilaments free of the silica membrane, due to easily accessible large surface areas and short diffusion lengths. In the best cases, spectroelectrochemical data corresponding to the variation of optical contrast recorded at 750 nm for successive interconversion of the emeraldine/leucoemeraldine system revealed ultrafast response speed (0.1 s for colouration and bleaching to reach 95% of maximum absorbance variation) and excellent cycling stability (100% of optical contrast maintained after 200 cycles between -0.2 and 0.3 V in 0.5 M H_2SO_4). The PANI nanofilaments are also promising for applications in other fields such as electrocatalysis and sensors or energy storage as supercapacitors.

Author contributions

WU: investigation, methodology, formal analysis, visualization, writing (original draft); GH: conceptualization, methodology, validation, supervision, writing (review & editing); NV: conceptualization, methodology, investigation, validation, supervision, writing (review & editing); AW: conceptualization, funding acquisition, validation, supervision, visualization, writing (original draft, review & editing).

Conflicts of interest

There are no conflicts to declare.

Acknowledgements

The authors are grateful to Dr Jaafar Ghanbaja (IJL – CNRS, Université de Lorraine) for TEM micrographs and to Mr Lionel Richaudeau (L2CM – CNRS, Université de Lorraine) for GISAXS measurements. WU acknowledges a PhD grant from the Université de Lorraine. This work was supported partly by the French PIA project "Lorraine Université d'Excellence" (grant N° ANR-15-IDEX-04-LUE).

Notes and references

[a] *Laboratoire de Chimie Physique et Microbiologie pour les Matériaux et l'Environnement (LCPME), UMR 7564, CNRS – Université de Lorraine, 405 rue de Vandoeuvre, Villers-lès-Nancy, F-54600, France.*
** Corresponding author fax: (+33) 3 83 27 54 44; e-mail: alain.walcarius@univ-lorraine.fr*

1 A. Walcarius, *Chem. Soc. Rev.*, 2013, **42**, 4098.
2 A. Walcarius, *Electroanalysis*, 2015, **27**, 1303.
3 M. Etienne, L. Zhang, N. Vila, A. Walcarius, *Electroanalysis*, 2015, **27**, 2028.
4 X. Yang, P. Qiu, J. Yang, Y. Fan, L. Wang, W. Jiang, X. Cheng, Y. Deng, W. Luo, *Small*, 2021, **17**, 1904022.
5 L. Zu, W. Zhang, L. Qu, L. Liu, W. Li, A. Yu, D. Zhao, *Adv. Energy Mater.*, 2020, **10**, 2002152.
6 C. Li, Q. Li, Y.V. Kaneti, D. Hou, Y. Yamauchi, Y. Mai, *Chem. Soc. Rev.*, 2020, **49**, 4681.
7 I.E. Rauda, V. Augustyn, B. Dunn, S.H. Tolbert, *Acc. Chem. Res.*, 2013, **46**, 1113.
8 J.C. Ndamanisha, L.-P. Guo, *Anal. Chim. Acta*, 2012, **747**, 19.
9 A. Walcarius, *Trends Anal. Chem.*, 2012, **38**, 79.
10 X. Bo, M. Zhou, Ming, in *Advanced Electrode Materials*, Eds. A. Tiwari, F. Kuralay and L. Uzun, Scrivener Publishing (2017), Chap. 6, pp. 213-241.
11 A. Walcarius, *Sensors*, 2017, **17**, 1863.
12 M. Hasanzadeh, N. Shadjou, M. de la Guardia, M. Eskandani, P. Sheikhzadeh, *Trends Anal. Chem.*, 2012, **33**, 117.
13 H. Rao, X. Wang, X. Du, Z. Xue, *Anal. Lett.*, 2013, **46**, 2789.
14 A. Walcarius, *Curr. Opin. Electrochem.*, 2018, **10**, 88.
15 F. Hoffmann, M. CorneliusJ. Morell and M. Froeba, *Angew. Chem. Int. Ed.*, 2006, **45**, 3216.
16 Y. Chen, J. Shi, *Adv. Mater.*, 2016, **28**, 3235.
17 V.B. Cashin, D.S. Eldridge, A. Yu, D. Zhao, *Environ. Sci. Water Res. Technol.*, 2018, **4**, 110.
18 D. Feng, J. Wei, M. Wang, Q. Yue, Y. Deng, A.M. Asiri, D. Zhao, *Adv. Porous Mater.*, 2013, **1**, 164.
19 G.J.A.A. Soler-Illia, P.C. Angelome, M.C. Fuertes, A. Calvo, A. Wolosiuk, A. Zelcer, M.G. Bellino, E.D. Martinez, *J. Sol-Gel Sci. Technol.*, 2011, **57**, 299.
20 C. Sanchez, C. Boissiere, D. Grosso, C. Laberty and L. Nicole, *Chem. Mater.*, 2008, **20**, 682.
21 K.C.-W. Wu, X. Jiang, Y. Yamauchi, *J. Mater. Chem.*, 2011, **21**, 8934.
22 V. Urbanova, A. Walcarius, *Z. Anorg. Allg. Chem.*, 2014, **640**, 537.
23 C. Mousty, A. Walcarius, *J. Solid State Electrochem.*, 2015, **19**, 1905.
24 F. Yan, X. Lin, B. Su, Analyst, 2016, 141, 3482.
25 P. Zhou, L. Yao, K. Chen, B. Su, *Crit. Rev. Anal. Chem.*, 2020, **50**, 424.
26 A. Walcarius, E. Sibottier, M. Etienne and J. Ghanbaja, *Nature Mater.*, 2007, **6**, 602.
27 A. Goux, M. Etienne, E. Aubert, C. Lecomte, J. Ghanbaja and A. Walcarius, *Chem. Mater.*, 2009, **21**, 731.
28 Z. Teng, G. Zheng, Y. Dou, W. Li, C.-Y. Mou, X. Zhang, A.M. Asiri and D. Zhao, *Angew. Chem. Int. Ed.*, 2012, **51**, 2173.
29 K.-C. Kao, C.-H. Lin, T.-Y. Chen, Y.-H. Liu, C.-Y. Mou, *J. Am. Chem. Soc.*, 2015, **137**, 3779.
30 M. Dutreilh-Colas, M. Yan, P. Labrot, N. Delorme, A. Gibaud and J.-F. Bardeau, *Surf. Sci.*, 2008, **602**, 829.
31 Y. Yamauchi, M. Sawada, M. Komatsu, A. Sugiyama, T. Osaka, N. Hirota, Y. Sakka and K. Kuroda, *Chem. Asian J.*, 2007, **2**, 1505.
32 E.K. Richman,T. Brezesinski and S.H. Tolbert, *Nature Mater.*, 2008, **7**, 712.
33 C. Robertson, R. Beanland, S. A. Boden, A. L. Hector, R. J. Kashtiban, J. Sloan, D. C. Smith, A. Walcarius, *Phys. Chem. Chem. Phys.*, 2015, **17**, 4763.
34 N. Vilà, J. Ghanbaja, E. Aubert, A. Walcarius, *Angew. Chem. Int. Ed.*, 2014, **53**, 2945.

35 N. Vilà, E. André, R. Ciganda, J. Ruiz, D. Astruc, A. Walcarius, *Chem. Mater.*, 2016, **28**, 2511.
36 W. Li, L. Ding, Q. Wang, B. Su, *Analyst*, 2014, **139**, 3926.
37 N. Vilà, P. de Oliveira, A. Walcarius, I.M. Mbomekallé, *Electrochim. Acta*, 2019, **309**, 209.
38 L. Sun, L. Zhou, F. Yan, B. Su, *Langmuir*, 2019, **35**, 14486.
39 M. Saadaoui, I. Fernandez, G. Luna, P. Diez, S. Campuzano, N. Raouafi, A. Sanchez, J.M. Pingarron, R. Villalonga, *Anal. Bioanal. Chem.*, 2016, **408**, 7321.
40 X. Lin, B. Zhang, Q. Yang, F. Yan, X. Hua, B. Su, *Anal Chem.*, 2016, **88**, 7821.
41 X. Lin, Q. Yang, F. Yan, B. Zhang, B. Su, *ACS Appl. Mater. Interfaces*, 2016, **8**, 33343.
42 N. Vilà, A. Walcarius, *Electrochim. Acta*, 2015, **179**, 304.
43 G. Giordano, N. Vilà, E. Aubert, J. Ghanbaja, A. Walcarius, *Electrochim. Acta*, 2017, **237**, 227.
44 S. Ahoulou, N. Vilà, S. Pillet, D. Schaniel, A. Walcarius, *Chem. Mater.*, 2019, **31**, 5796.
45 J. Wang, N. Vilà, A. Walcarius, *ACS Appl. Mater. Interfaces*, 2020, **12**, 24262.
46 S. Saint-André, F. Albanese, G.J.A.A. Soler-Illia, M. Tagliazucchi, *Phys. Chem. Chem. Phys.*, 2019, **21**, 2743.
47 A. Goux, J. Ghanbaja, A. Walcarius, *J. Mater. Sci.*, 2009, **44**, 6601.
48 L. Lu, L. Zhou, J. Chen, F. Yan, J. Liu, X. Dong, F. Xi, P. Chen, *ACS Nano*, 2018, **12**, 12673.
49 P.N. Bartlett, R. Beanland, J. Burt, M.M. Hasan, A.L. Hector, R.J. Kashtiban, W. Levason, A.W. Lodge, S. Marks, J. Naik, A. Rind, G. Reid, P.W. Richardson, J. Sloan, D.C. Smith, *Nano Lett.*, 2018, **18**, 941.
50 M.A. del Valle, M. Gacitúa, F.R. Díaz, F. Armijo, R. del Río, *Electrochem. Commun.*, 2009, **11**, 2117.
51 M.A. del Valle, A. Ramos, M. Antilen, L. Hernandez, G. Arteaga, F. Diaz and G. Louarn, *Electrochemistry*, 2014, **82**, 146.
52 S.M. Fonseca, T. Moreira, A.J. Parola, C. Pinheiro, C.A.T. Laia, *Sol. Energy Mater. Sol. Cells*, 2017, **159**, 94.
53 H. Kang, H. Lee, J. Kwak, *J. Korean Electrochem. Soc.*, 2011, **14**, 22.
54 L. Ding, W. Li, Q. Wang, Q. Sun, Y. He, B. Su, *Chem. Eur. J.*, 2014, **20**, 1829.
55 M.A. del Valle, L.A. Hernández, A.M. Ramírez, F.R. Díaz, *Ionics*, 2016, **23**, 191.
56 A.M.R. Ramírez, M. Gacitúa, E. Ortega, F.R. Díaz, M.A. del Valle, *Electrochem. Commun.*, 2019, **102**, 94.
57 A. Gamero-Quijano, C. Karman, N. Vilà, G. Herzog, A. Walcarius, *Langmuir*, 2017, **33**, 4224.
58 M.A. del Valle, L.A. Hernández, F.R. Díaz, A. Ramos, *Int. J. Electrochem. Sci.*, 2015, **10**, 5152.
59 L.A. Hernández, M.A. del Valle, F.R. Díaz, D.J. Fermín, T.A.G. Risbridger, *Electrochim. Acta*, 2015, **166**, 163.
60 W. Ullah, G. Herzog, N. Vilà, A. Walcarius, *Electrochem. Commun.*, 2021, **122**, 106896.
61 N.-R. Chiou, C. Lu, J. Guan, L.J. Lee, A.J. Epstein, *Nat. Nanotechnol.*, 2007, **2**, 354.
62 W. Zhong, J. Deng, Y. Yang, W. Yang, *Macromol. Rapid Commun.*, 2005, **26**, 395.
63 L. Jiang, Z. Cui, *Polym. Bull.*, 2006, **56**, 529.
64 J. Lyskawa, D. Bélanger, *Chem. Mater.*, 2006, **18**, 4755.
65 A. Subrata, A. Veksha, Z.Y. Pong, G. Lisak, R.D. Webster, *ChemElectroChem*, 2020, **7**, 3368.
66 A. Vacca, M. Mascia, S. Rizzardini, S. Palmas, L. Mais, *Electrochim. Acta*, 2014, **126**, 81.
67 K. Darowicki, J. Kawula, *Electrochim. Acta*, 2004, **49**, 4829.
68 J. Stejskal, R.G. Gilbert, *Pure Appl. Chem.*, 2002, **74**, 857.
69 A. Yazdanpanah, A. Ramedani, A. Abrishamkar, P.B. Milan, Z.S. Moghadan, N.P.S. Chauhan, F. Sefat, M. Mozafari, in *Fundamentals and Emerging Applications of Polyaniline*, Eds. M. Mozafari and N.P.S. Chauhan, Elsevier (2019), Chap. 6, pp. 105-119.
70 J. Cheng, S.J. Rathi, P. Stradins, G.L. Frey, R.T. Collins, S.K.R. Williams, *RSC Adv.*, 2014, **4**, 7627.
71 D. Ge, L. Yang, Z. Tong, Y. Ding, W. Xin, J. Zhao, Y. Li, *Electrochim. Acta*, 2013, **104**, 191.
72 J.W. Schultze, A. Thyssen, *Synth. Met.*, 1991, **43**, 2825.
73 P. Yu, C. Li, X. Guo, *J. Phys. Chem. C*, 2014, **118**, 10616.
74 S. Zhang, J. Ren, S. Chen, Y. Luo, X. Bai, L. Ye, F. Yang, Y. Cao, *J. Electroanal. Chem.*, 2020, **870**, 114248.
75 M. Jamdegni, A. Kaur, *Thin Solid Films*, 2020, **714**, 138373.
76 X. Huang, Q. Niu, S. Fan, Y. Zhang, *Chem. Eng. J.*, 2021, **417**, 128126.
77 M. Etienne, Y. Guillemin, D. Grosso, A. Walcarius, *Anal. Bioanal. Chem.*, 2013, **405**, 1497.
78 T. Nasir, G. Herzog, L. Liu, M. Hébrant, C. Despas, A. Walcarius, *ACS Sensors*, 2018, **3**, 484.
79 A. Watanabe, K. Mori, Y. Iwasaki, Y. Nakamura, S. Niizuma, *Macromolecules*,1987, **20**, 1793.
80 S. Zhang, S. Chen, F. Hu, R. Xu, B. Yan, M. Jiang, Y. Gu, F. Yang, Y. Cao, *Sol. Energy Mater. Sol. Cell.*, 2019, **200**, 109951.
81 R.C. Silva, M.V. Sarmento, F.A.R. Nogueira, J. Tonholo, R.J. Mortimer, R. Faez, A.S. Ribeiro, *RSC Adv.*, 2014, **4**, 14948.
82 S. Zhang, G. Sun, Y. He, R. Fu, Y. Gu, S. Chen, *ACS Appl. Mater. Interfaces*, 2017, **9**, 16426.
83 S. Mishra, S. Lambora, P. Yogi, P.R. Sagdeo, R. Kumar, *ACS Appl. Nano Mater.*, 2018, **1**, 3715.
84 Y. Wang, S. Xiong, X. Wang, J. Chu, R. Zhang, M. Gong, B. Wu, M. Qu, Z. Li, Z. Chen, *Polym. J.*, 2020, **52**, 783.
85 A. Habib, S.P. Maheshwari, *J. Electrochem. Soc.*, 1989, **136**, 1050.
86 M. Fabretto, T. Vaithianathan, C. Hall, P. Murphy, P.C. Innis, J. Mazurkiewicz, G.G. Wallace, *Electrochem. Commun.*, 2007, **9**, 2032.
87 L. Wang, Y. Ye, Y. Shen, F. Wang, X. Lu, Y. Xie, S. Chen, H. Tan, F. Xu, Y. Song, *Sens. Actuators B Chem.*, 2014, **203**, 864.
88 L. Liu, J. Guo, L. Ding, *Electroanalysis*, 2021, **33**, 2048.
89 N. Hui, F. Chai, P. Lin, Z. Song, X. Sun, Y. Li, S. Niu, X. Luo, *Electrochim. Acta*, 2016, **199**, 234.
90 N. Hui, J. Wang, A. Liang, M. Jiang, *Electroanalysis*, 2016, **28**, 279.
91 K. Wang, H. Wu, Y. Meng, Z. Wei, *Small*, 2014, **10**, 14.
92 X. Gao, H. Zhang, H. Yue, F. Yao, X. Zhang, E. Guo, Y. Ma, Z. Wang, Y. Wang, *ChemistrySelect*, 2020, **5**, 11004.
93 C. Sanchis, M.A. Ghanem, H.J. Salavagione, E. Morallón, P.N. Bartlett, *Bioelectrochem.*, 2011, **80**, 105.
94 Y. Zhang, W. Chu, Q. Zhou, S. Li, N. Li, J. Zheng, *J. Electroanal. Chem.*, 2016, **775**, 105.
95 J. Wang, N. Vilà, A. Walcarius, *Electrochim. Acta*, 2021, **366**, 137407.